
Sensor fusion for complex articulated body tracking applied in rowing

Journal of Sports Engineering and
Technology
000(00):1–13
©The Author(s) 2010
Reprints and permission:
sagepub.co.uk/journalsPermissions.nav
DOI:doi number
<http://jms.sagepub.com>

E. Ruffaldi*, L. Peppoloni, A. Filippeschi
PERCRO Laboratory, Scuola Superiore Sant'Anna, Pisa, Italy

Author name

Affiliation

Abstract

The paper presents a sensor fusion model for integrating wearable inertial measures with sensors in the environment. This approach is designed and tested to support body motion tracking of rowing in indoor and outdoor environment. The paper presents the approach based on a complex kinematic model and unscented Kalman filtering. The approach is validated in an in-door setup based on the SPRINT rowing system by comparison against results obtained from a commercial motion capture system, thus providing future directions for the assessment of rowers' performance on an instrumented boat.

Keywords

motion reconstruction, sensor fusion, rowing, kalman filter, kinematics

1. Introduction

The quantitative assessment of subject performance is one of the basic elements of technology-assisted training and self-evaluation of performance in the context of real and virtual environments [1, 2]. The measurement technologies that support this assessment have been introduced in several human and sport activities, provided their reliability and minimal disruption of performance.

A specific aspect of interest, that has the potential of supporting new types of motor training protocols, is the tracking of limb motion in outdoor environments. While body tracking has been traditionally based on optical systems [3], outdoor tracking can take advantage of wearable inertial based measurement systems. Wearable systems present interesting opportunities for the activities in which the working area is not specified. In addition, camera systems can suffer from occlusion problems when the subject interacts with external devices.

The hypothesis of this work is to provide an efficient and precise motion tracking by combining different sensor types and by exploiting knowledge about the kinematic chains involving the human body and the surrounding instruments. This

* Corresponding author; e-mail: e.ruffaldi@sssup.it

hypothesis is specifically aimed at the case of inertial wearable units fused with minimally instrumented oars in a rowing boat.

The assessment of the approach is performed in an indoor setup with the SPRINT research ergometer whose dynamics has been previously validated against measurements gathered on an instrumented boat [4]. The motion estimation based on the proposed approach is compared against measures gathered on the SPRINT system by means of an optical motion capture system.

The manuscript is organized as follows. The state of the art in motion reconstruction is discussed, then the material and methods section discusses the kinematic model and the reconstruction approaches and the setup for simulated and real experiments. The results of simulation and real tests are presented. The paper is closed by a discussion and conclusions.

2. Background

The approaches for reconstruction of motion in outdoor environment can be categorized along two directions: the placement of the sensors and the technology employed. The grounded placement of sensors is the typical solution for optical motion capture system, either marker-based or marker-less. Unfortunately, the grounded placement is limited in the workspace and can be affected by outdoor conditions like visibility or lighting conditions. A different approach is provided by wearable sensors that have two main drawbacks: first the possible encumbrance and limitation of subject motion, second the typical lack of absolute positioning. The technology employed can span from optical solutions, both grounded and wearable, to inertial solutions, or hybrid approaches.

The most adopted solution for wearable sensing is based on inertial measures thanks to the advancements in MEMS that have reduced the size and improved the precision of this type of technology. In some cases, the inertial technology is combined with other approaches as follows: [5] combined inertial with ultrasonic devices for portable motion tracking of the limbs; [6] integrated a body worn camera for reducing drifting and uncertainty of inertial measures.

In sports in which the subject performs his activity interacting with a structure, such the boat in rowing, it is possible to combine sensors mounted on the structure with wearable sensors. For the rowing case several research efforts have been dedicated to create instrumented boats for assessing the performance of the rowers by measuring the dynamics of the boat and the motion of the oars. Recent examples are the SonicSeat [7], that employs ultrasonic sensors for seat tracking, or [8] and [9] that tracks seat and oars by means of inertial units.

The purpose of monitoring performance in rowing relies on the application of motor control and feedback techniques for obtaining quantitative assessment of rower's performance, focused on technique training [2] or energy management [10] among the others.

The present work covers one aspect not previously addressed, that is the tracking of the motion of the upper limbs for complementing the performance assessment typically performed with the measure of seat and oar motion. In comparison to camera-based setups this approach is suitable also for outdoor measurements with minimal encumbrance for the subject.

Human motion tracking based on IMUs has been widely studied in the last decade. While being self contained, and unobtrusive, the main drawback of this approach is the impossibility of directly integrating IMUs measurements because of drifts affecting data. Several filtering and sensor fusion techniques have been applied to solve this problem, especially exploiting Bayesian filters. Early models typically exploited linear filters such as the Kalman Filter (KF), neglecting kinematic constraints between the limb considered and estimating every limb orientation independently. This kind of approach has been applied by Zhou in [11], where the author estimates the human limb attitude through the gravity and Earth magnetic field, corrected with a linear KF. In that work, only one degree of freedom (DoF) for the arm is considered, obtaining a position error less than 1 cm, although accuracy is sensitive to measurement accuracy and physical dimensions of all corresponding segments. Recent approaches usually exploit nonlinear Bayesian filters, such as Extended Kalman Filter (EKF), Unscented Kalman Filter (UKF) and Particle Filters (PF). Thanks to the capability of these algorithms to

manage more complex models, the human body is modeled as a kinematic chain, taking into account also kinematic constraints. Several algorithms and possible models have been presented. Yun and Bachmann [12] combine a QUEST algorithm [13] with an EKF to estimate the quaternions representing limbs orientation. They propose a 3 DoFs, validated through comparison with tilt table measurements. Roetenberg et al. [14] track the human full body, estimating and correcting the orientation errors obtained by integrating inertial measurements with an EKF. A different approach is proposed by El Gohary and McNames [15], in which they exploit a 5 DoFs model for the human upper limb and an UKF, estimate joint angles, velocities and accelerations. The human shoulder is modeled with a spherical joint, while two rotational joints model the elbow. The system is validated through comparison with an optical tracking system. Results obtained show an average RMS error of less than 8° and a cross correlation coefficient $r \geq 0.95$ for joints angles. Peppoloni et al. [16] apply a similar approach presenting a more complex kinematic model. The authors exploit the UKF to estimate joint variables for a 7 DoFs model of the human upper limb that include the displacement of the humerus head due to the scapula motion. The Bayesian Filtering approach has been pushed even further by Ruffaldi et al. in [17], where the authors present a new filtering algorithm based on Probabilistic Graphical Models (PGM) to estimate human upper limb joint variables. The algorithm allows a better representation of the actual independence relationships between the variables considered. The results show a slight improvement compared to the classical UKF approach.

3. Materials and Methods

This section discusses the sensor fusion approach proposed by this work. At first the kinematic model employed for describing the rower are presented, then the sensor model adopted for capturing the motion. These two models are then used for constructing a sensor fusion problem involving state variables with their dynamics, and the measurement model. The nonlinearity of the measurement model requires a nonlinear filter, such as EKF, UKF or particle filter. We selected UKF as it estimates well both the mean and the covariance of the state variables when transformed by a nonlinear function (see [18]), and it requires fewer computational resources with respect to particle filters. As it will be discussed in the kinematic model and the measurement model (Sections 3.4 and 3.1) the resulting Kalman problem has a 37 variables state (3×11 dynamic and 4 non-dynamic variables), and an observation model whose output's dimension is 58 (9×5 inertial, 1 joint, 3×2 positions, 3×2 axes). Finally the methods used for the evaluation of the system are proposed, as simulation and as real cases. In the following the notation reported in table 1 will be used.

Table 1. List of Symbols used in the text

Symbol	Unit	Description
ϕ	rad	oar rotation along the direction of motion of the boat
α	rad	oar vertical rotation
θ	rad	oar rotation along the axis
i	index	frame index
p	index	parent frame index
A_i^p	affine matrix	transformation from frame i to parent frame
R_i^p	rotation matrix	rotation part of A_i^p
T_i	affine matrix	global transformation from frame i to reference frame
q_i	rad or m	joint variable
x_i	state	kalman state variable
v_j	m/s	velocity vector
\dot{v}_j	m/s^2	acceleration vector
ωx_j	rad/s	angular velocity vector
$\dot{\omega}_j$	rad/s^2	angular acceleration vector
g_j	m/s^2	gravity vector in frame j
m_i	tesla	magnetic field vector
T_s	s	sample time
$l_{cl}, l_{ua}, l_{fa}, l_{ha}$	m	lengths of relevant body parts

3.1. Kinematic Model

The model describes the interaction of the rower with the boat elements, covering the trunk and the upper limbs of the rower while interacting with the boat elements. The model can be described as a graph of kinematic chains of rigid links rooted on the boat structure, describing the motion of the seat, the trunk, the two upper limbs, and the two oars, assuming, in this case, a sculling technique.

The model is a closed kinematic chain with two loops that has to be cut transforming the graph representation in a tree. In particular, it has been chosen to cut the chain at the attachment between the hands and the oars, being the natural interface between the human and the boat. In this way the system is represented by four chains, one for each limb, one for each oar.

The chains for the oars are made by three rotational joints centered in the oar lock, with a fixed translation with respect to the chosen root on the boat structure. The convention adopted for the angles of the oars is in line with the one adopted by the authors in previous paper [4]: the ϕ angle represents the rotation along the direction of motion of the boat, with the zero position at the center, positive sign away from the rower; the α angle is the vertical rotation, with the zero when parallel to the water, and positive upward; finally the θ angle that is the rotation on the axis of the oar, positive rotating away from the body.

The kinematic model for the rower's body balances the complexity of reconstruction with the information that is useful for characterizing the rower performance. In particular the trunk has been simplified by means of a single rotation point at the pelvis: the complexity of representing the bending of the back is left for future investigation starting from the approach described in this work. Each limb is described by a total of 7 DoFs: three for the shoulder, two for the elbow and two for the hand. The convention adopted for the limbs' angles are in line with the anatomical notation and follows the previous works of the authors [16] with the addition of the hand DoFs. Finally, the trunk of the rower is also connected to the boat structure by means of a prismatic joint describing the motion of the seat sliding on the guide.

All four kinematic chains have been described using the Denavit-Hartenberg (D-H) notation [19], with a total of 22 DoFs: 7 DoFs per arm, 3 DoFs per oar, 1 DoF for the seat, 1 DoF for the trunk rotation at the pelvis.

Table 2 presents the parameters of the model following the adopted convention: each frame is described in terms of the parent frame, and the four D-H parameters. All the frames are associated to rotational joints, except for the one related to the seat. Equation 1 shows the constant transformation to get the oars' base frames from the root frame. Figure 1 shows a 3D representation of the kinematic model presented in the neutral "N-pose" with the axis of reference shown for the terminal frames. The parameters required to determine the kinematic model (e.g. arm lengths) are manually measured out after the setup of the system.

The adoption of the D-H notation is connected with the standard description of the transformations and dynamic attributes of each frame i as a function of the parent frame p , as they are used for the reconstruction. In the following A_i^p is the transformation from the frame i to the parent frame p induced by the parameters and the joint variables, $T_i = A_i^0$ is the global transformation from the frame i to the root frame. The velocities and accelerations of a frame i expressed in the frame j are described as $v_i^j, \omega_i^j, \dot{v}_i^j$ and $\dot{\omega}_i^j$. When the apex is not reported in these variables it corresponds to the pedex. That is ω_i is the angular velocity of the frame i expressed in the same frame.

$$A_{18}^0 = \begin{bmatrix} -1 & 0 & 0 & \\ 0 & 0 & 1 & r_{0,18}^0 \\ 0 & 1 & 0 & \\ 0 & 0 & 0 & 1 \end{bmatrix} \quad A_{23}^0 = \begin{bmatrix} -1 & 0 & 0 & \\ 0 & 0 & 1 & r_{0,22}^0 \\ 0 & 1 & 0 & \\ 0 & 0 & 0 & 1 \end{bmatrix} \quad (1)$$

Table 2. DH table and joint correspondence. $l_{cl}, l_{ua}, l_{fa}, l_{ha}$ are clavicle, upper arm, forearm length, and hand length respectively, with the arm in the apex. l_b is the length of the back, l_{oar}^R, l_{oar}^L is the length of the right and left oar respectively.

Frame	Parent	a	α	d	θ	Joint
1	0	0	$-\pi/2$	q_1	$\pi/2$	Seat (prismatic)
2	1	l_b	$-\pi/2$	l_{cl}^R	q_2	R Back
3	2	0	$\pi/2$	0	$q_3 - \pi/2$	R Shoulder Abduction
4	3	0	$-\pi/2$	0	$q_4 - \pi/2$	R Shoulder Rotation
5	4	l_{ua}^R	0	0	$q_5 - \pi/2$	R Shoulder Flexion
6	5	0	$\pi/2$	0	$\pi/2 + q_6$	R Elbow Flexion
7	6	0	$-\pi/2$	l_{fa}^R	q_7	R Elbow Rotation
8	7	0	$-\pi/2$	0	$q_8 - \pi/2$	R Hand Abduction
9	8	$-l_{ha}^R$	0	0	q_9	R Hand Flexion
10	1	l_b	$\pi/2$	$-l_{cl}^L$	q_2	L Back
11	10	0	$\pi/2$	0	$q_{10} - \pi/2$	L Shoulder Abduction
12	11	0	$-\pi/2$	0	$\pi/2 + q_{11}$	L Shoulder Rotation
13	12	l_{ua}^L	0	0	$q_{12} - \pi/2$	L Shoulder Flexion
14	13	0	$\pi/2$	0	$\pi/2 + q_{13}$	L Elbow Flexion
15	14	0	$-\pi/2$	l_{fa}^L	q_{14}	L Elbow Rotation
16	15	0	$\pi/2$	0	$q_{15} - \pi/2$	L Hand Abduction
17	16	$-l_{ha}^L$	0	0	q_{16}	L Hand Flexion
18	0		see A_{18}^0 in equation 1			R Oar Base
19	18	0	$-\pi/2$	0	q_{18}	R Phi
20	19	0	$\pi/2$	l_{oar}^R	$q_{19} - \pi/2$	R Alpha
21	20	0	0	0	q_{20}	R Rotation
22	0		see A_{22}^0 in equation 1			L Oar Base
23	22	0	$-\pi/2$	0	q_{18}	L Phi
24	23	0	$\pi/2$	l_{oar}^L	$q_{19} - \pi/2$	L Alpha
25	24	0	0	0	q_{20}	L Rotation

3.2. Sensor Model

The sensor model used for body tracking comprises a set of sensors of different nature, placed on the boat and on the rower's body. For the analysis performed in this work the sensing of the boat is made by two elements: the seat is assumed to be tracked in position, for example using a wire draw encoder, while the oars are sensed in the α and ϕ angles by means of an optical encoder or a potentiometer. This selection of sensors is useful for the experimental testing, while not affecting the general method discussed in the paper. In particular these sensors are the ones present on the SPRINT ergometer platform, and on the instrumented boat used in previous work [4]. It has to be noted that the oars are not sensed along the θ axis. Overall the boat sensors contribute with 5 scalar signals. The sensing on the rower's body is modeled by means of one inertial unit on the trunk in the midpoint between the scapula, and two inertial units for each upper limb, on the arm and the forearm. Each inertial unit is equipped with an accelerometer, a gyroscope and a magnetometer, thus being a full 9-axis sensor. Therefore, 45 scalar signals are available in the whole the body. The combination of the boat and body-worn sensors totals 50 scalar signals. Table 3 shows the sensors employed in the model and their connection with the kinematic model frames. The setup we propose is minimally invasive, as IMU mass is below 30g and is suitable for both indoor and outdoor rowing.

Table 3. Table of sensors used for the setup and their relationship with the joints

Sensor	Frame	Sensor Type	Name
1	2	Inertial 9D	Back
2	5	Inertial 9D	R Upperarm
3	7	Inertial 9D	R Forearm
4	13	Inertial 9D	L Upperarm
5	15	Inertial 9D	L Forearm
6	1	Position 1D	Seat
7	19	Encoder 1D	R Phi
8	20	Encoder 1D	R Alpha
9	23	Encoder 1D	L Phi
10	24	Encoder 1D	L Alpha

3.3. System Dynamics

The chosen dynamics defines the state space model of the reconstruction process. Only the joints defining the user motion are included in the state. In particular we include, with reference to Table 2, $[q_1, \dots, q_{16}]$. The state model for the joints $q_1, \dots, q_7, q_{10}, \dots, q_{14}$ is composed of joint angles, velocities and accelerations, obtaining for each joint

$$x_i = [q_i, \dot{q}_i, \ddot{q}_i]^T \quad i = 1, \dots, 7, 10, \dots, 14. \quad (2)$$

Since inertial sensors are placed only on the user's upper arms and forearms, the velocities and accelerations of the two hands' DoFs (namely q_8, q_9, q_{15}, q_{16}) are not included in the states, resulting in:

$$x_i = q_i \quad i = 8, 9, 15, 16. \quad (3)$$

Starting from the generic formulation of the state space model with additive noise for discrete systems:

$$x(k+1) = f(x(k)) + \nu_k \quad (4)$$

where $f(\cdot)$ is a potential nonlinear function and ν_k is the process Gaussian white noise. Once defined the system sample time as T_s , the state model equations for each joint results:

$$\begin{bmatrix} q_i(k+1) \\ \dot{q}_i(k+1) \\ \ddot{q}_i(k+1) \end{bmatrix} = \begin{bmatrix} 1 & T_s & \frac{1}{2}T_s^2 \\ 0 & 1 & T_s \\ 0 & 0 & 1 \end{bmatrix} \begin{bmatrix} q_i(k) \\ \dot{q}_i(k) \\ \ddot{q}_i(k) \end{bmatrix} + \nu_i(k) \quad (5)$$

where the joint acceleration dynamics is modeled as a random walk process. The resulting block of the covariance matrix is:

$$Q_i = \begin{bmatrix} \frac{1}{2}T_s^2 \\ T_s \\ 1 \end{bmatrix} \begin{bmatrix} 1 & T_s & 1 \\ \frac{1}{2}T_s^2 & T_s & 1 \end{bmatrix}, \quad (6)$$

The complete state space model is obtained by assembling the equations 5 and the covariance matrix blocks 6.

3.4. Measurement Model

The measurement model relates the sensor measurement to the state variables. The overall measures are expressed by the variable z defined from the $h(x)$ as follows:

$$z(k) = h(x(k)) + \eta_k \quad (7)$$

Each sensor contribution is based on the same equations employed in the previous work [16] with three key differences. First the kinematic structure considered here is a general tree with multiple chains, and the notation for the sensors has to be modified: every sensor, as from Table 3, refers to a link l against which it is placed, resulting in a parent frame p and an associated state variable s that depends on the D-H Table 2. For example sensor 2 is attached on the upper arm corresponding to the frame $l = 5$, that has parent $p = 4$ and joint variable q_5 .

For the inertial sensors (1..5 in Table 3) the contributions to the measurement function h is:

$$h_i(x) = [\omega_i, \dot{v}_i, m_i]^T \quad (8)$$

where three elements are present: the angular velocity (ω), the linear acceleration comprising the gravity vector (\dot{v}) and the Earth magnetic field (m). This equation leads to the following governing equations, based on the above notation:

$$\begin{aligned} \omega_i &= R_p^i(\omega_p + \dot{q}_s z_0) \\ \dot{\omega}_i &= R_p^i(\dot{\omega}_p - \dot{q}_s S(z_0)\omega_p + \ddot{q}_s z_0) \\ \dot{v}_i &= R_p^i \dot{v}_p - S(r_{p,i}^i)\dot{\omega}_i + S(\omega_i)^2 r_{p,i}^i + g_i \\ g_i &= R_p^i g_p \\ m_i &= R_p^i m_p \\ z_0 &= [0, 0, 1]^T \end{aligned} \quad (9)$$

where we use the convention for vectors with pedex as the entity, and the apex as the reference system. For example $r_{p,i}^i$ represents the vector connecting the origin of the frame p to the origin of the frame i written in the frame i . When the apex is missing it is the same as the pedex: e.g. ω_p^i is the angular velocity of frame p expressed in the reference system of sensor i . R_i^j expresses the transformation from a vector in reference system i to reference system j . The local gravity contribution g_i is contained in \dot{v}_i . We also remember the property $S(\omega)^2 = -S(\omega)S(\omega)^T$, where $S(v)$ is the skew-matrix obtained from vector v . The second difference is in the nature of the sensor employed for the seat (sensor 6) and the oar encoders. The motion of the seat is prismatic, and the wired sensor used for the measurement provides directly the associated variable.

This means that the contribution of this sensor to the h function is:

$$h_6(x) = q_1 \quad (10)$$

Similarly the oar encoders provide direct measures of the α and ϕ angles for the contribution $h_7 \dots h_{10}$. For all these sensors the measurement covariance is very low. The third improvement of this work is in the management of the closed kinematic chains as shown in Section 3.1. As discussed above the kinematic chains comprising the arm and the oar, are cut at the attachment between the hand and the oar handle. The closure of the chain is enforced by introducing two virtual sensors for every oar that provide an estimate of the position of the hand called r_p, r_z and l_p, l_z : the first is an estimate of the position in global coordinates of the attachment point of the hand on the oar, the second is the axis of the oar directed toward the handle. The measurements for those virtual sensors are calculated based on the α and ϕ angles measured by the encoders. From the convention adopted for the hand and the oar, the matching axes correspond to the local axis Y for the hand and the X axis for the oar. This leads to the following formulation of the constraint by extracting the cosine directors of the global transformation matrices T_i and the translation component of the transformation:

$$(T_9)_z = (T_{21})_z \quad (11)$$

$$r_{0,9}^0 = r_{0,21}^0 \quad (12)$$

$$(T_{17})_z = (T_{25})_z \quad (13)$$

$$r_{0,17}^0 = r_{0,25}^0 \quad (14)$$

The virtual sensors are an elegant way to add new constraints combining measurement equations and the associated virtual measurements. In this case these constraints are enforced by adding four further equations to the measurement model:

$$h_{rp} = r_{0,9}^0 - r_{0,21}^0 = 0 \quad (15)$$

$$h_{rz} = (T_9)_z - (T_{21})_z = 0 \quad (16)$$

$$h_{lp} = r_{0,17}^0 - r_{0,25}^0 = 0 \quad (17)$$

$$h_{lz} = (T_{17})_z - (T_{25})_z = 0 \quad (18)$$

The measurement function is obtained by combining the functions of the seat sensor, the inertial sensors of the arms (e.g. $h_1 \dots h_6$) and the constraints obtained from the closure of the kinematic chain (i.e. $h_{rp}, h_{rz}, h_{lp}, h_{lz}$).

4. Results

4.1. Simulated Inertial Sensors Experiment

The first assessment of the proposed approach is based on simulated measures of IMUs that are based on indoor motion recordings. The comparison of the simulated data against the results of the estimation allows us to get the exact estimation error. However, this validation method raises the issue of the consistence of the simulated data with respect to the real task. To address this issue we generated simulated data from real data gathered during an indoor capturing session.

We collected data from an expert rower (male, aged 24, medalist at 2009 Under 23 Rowing World Championships) who was asked to row on the SPRINT system focusing on the technique. The SPRINT system consists of a platform fixed to the ground including two oars, a sliding seat and a foot-stretcher similar to outdoor rowing shells [20]. The platform was equipped with encoders that capture oars' rotations with respect to the platform and the displacement of the seat. The force that is exerted on the oars is estimated according to the oar motion as explained in [21] and can be widely regulated to meet requirements of sculling and sweep rowing. The rower was equipped with markers on the following body landmarks (both

Sensor	Acceleration [$m/s^2 \cdot 10^{-3}$]	Angular speed [$rad/s^2 \cdot 10^{-3}$]	Magnetic Field [μT]
IMU1	7.16	8.36	1.242
IMU2	5.18	11.09	1.167
IMU3	3.66	6.75	1.028
IMU4	4.24	4.35	0.951
IMU5	1.92	4.46	0.863

Table 4. Standard deviations for the generation of the sensor simulated measurement.

left and right side): hips, sternum breastbone, shoulder acromion, lateral and medial humeral epicondyles, ulna and radius styloid process. Markers' positions were captured by a commercial motion capture setup (Vicon with 7 MX2 cameras), data were processed by the Vicon Nexus software and made available on the network via UDP to reconstruct rower's trunk and arm motion, as well as the seat motion. Both SPRINT and Vicon data were recorded by using the Matlab Simulink[®] software that ran at 125 Hz.

The markers trajectories were pre-processed by filling the capturing gaps by means of spline interpolant and filtered with a zero-phase forward reverse IIR lowpass filter whose cutoff frequency is 10 Hz. Marker data were then processed according to [22] to obtain the joints variables of the kinematic model described in Section 3.1. The obtained joint variables were the goal of the reconstruction based on the presented algorithm. We then introduced virtual sensors on the rower body. We placed them according to the setup shown in Section 3.1 by setting the homogeneous matrices representing their pose with respect to their parent limb. We then simulated their measurements from the generated joint motion by adding a Gaussian white noise. The noise standard deviation was calculated based on the data that we gathered in steady conditions from the Invensense IMUs MPU9150 (Invensense, Borregas Ave Sunnyvale, CA, USA) that we use for motion reconstruction. Table 4.1 reports the standard deviation that we obtained from the five sensors that were used. We also simulated the possibility of unknown biases on the accelerometers and gyroscopes measurements (see table 5 for bias details).

Since the boat inertia is not addressed in the reconstruction model, we added the effect of boat velocity and acceleration to the virtual measures in order to investigate how neglecting the boat motion influences the estimation. Boat motion was calculated according to a 2 DoFs boat dynamics model obtained in previous work [4] that was fed with the measurements from the oars.

4.2. Inertial motion capture experiment

The proposed approach is evaluated in a motion reconstruction task performed on the SPRINT system together with a wearable inertial system and validated against the measurement of a motion capture system. The test setup is shown in Figure 2.

The experiment was performed on the SPRINT system with the seat position provided by a wire potentiometer Posiwire[®] ws31C. This type of acquisition device is the same as employed for the instrumentation of a boat [4]. The rest of the SPRINT setup is the same of the previous experiment.

The participant was instrumented with 5 IMUs MPU9150 placed on the back, upper arm and fore arm (see figure 2). The IMUs communicated via Bluetooth to an acquisition pc. The reference information was provided by the marker based motion capture as explained in Section 4.1. In this case data were not sent to Matlab Simulink but processed by the Nexus software (Vicon Oxford 14 Minns Business Park West Way Oxford, UK) and saved in the pc running the Vicon Nexus software. Data capturing frequency was 100 Hz for all the devices.

In this experiment the participant was instructed to perform a three-step calibration procedure needed to compute the inertial sensors orientation and calibrate the magnetometers. Then, he was asked to perform multiple sequences of rowing

strokes, while being tracked both by the optical and inertial tracking systems. Data were captured for two 40 seconds trials in which the participant was asked to focus on rowing technique.

For this experiment the joints of the rower were reconstructed by both the commercial motion capture system and the proposed technique. The quality assessment is based on the comparison of the estimation of the position of selected optical markers. This approach is alternative to the comparison based on the joint angles, and it has the advantage of removing from the comparison the errors due to the kinematic reconstruction based on the motion capture data, such as subject calibration and kinematic fitting. The estimated positions have been compared using root mean square error (RMSE) and coefficient of correlation.

4.3. Results on Simulated Inertial Sensors

These are the results of the simulated inertial sensors based on the recorded motion data. The reconstruction was based on the model described in Section 3.4 in which the oar handle pose was not available. Figure 3 shows the reconstructed joint variables against the real ones. Table 5 presents four cases combining the effects of boat inertia and additional sensor noise. For each case two measures are reported: the root mean square error (RMSE) for each joint, expressed in meters for the prismatic joint and in degrees for the rotoidal, and then the correlation between the trajectories.

However, in this test we knew exactly the pose of each sensor with respect to its parent limb. Therefore we made another experiment involving real sensors measurements.

Table 5. RMSE and correlation coefficient for all the joints in the kinematic model with synthetic sensors measurements. Four simulation conditions are reported and identified as X - Y. X is related to the simulated boat, when X is S it means that the boat acceleration is zero, when X is B boat acceleration is estimated from the rower motion and the forces on the oar. Y is related to an unknown bias on the accelerometer and gyroscope measurements, when Y is NB both biases are zero, when Y is B the accelerometer bias is 0.01 m/s^2 on each component and the gyroscope bias is 0.01 rad/s on each component. These bias values are ten times the biases that we gathered from the IMUs in static condition. The unit of measure of the joint is reported in brackets: all joints except the first are rotoidal and the error is expressed in degrees, the first is prismatic and the error is expressed in meters.

Joints	RMSE				Correlation r			
	S - NB	B - NB	S - B	B - B	S - NB	B - NB	S - B	B - B
$q_1 [m]$	0.016	0.018	0.020	0.021	0.997	0.996	0.996	0.996
$q_2 [deg]$	24.41	24.31	26.30	26.41	0.423	0.425	0.344	0.330
$q_3 [deg]$	3.32	3.11	3.39	3.22	0.972	0.974	0.968	0.971
$q_4 [deg]$	4.88	5.17	5.33	4.69	0.996	0.994	0.994	0.993
$q_5 [deg]$	9.46	9.57	7.93	8.79	0.998	0.999	0.997	0.999
$q_6 [deg]$	10.78	10.76	10.77	11.01	0.983	0.982	0.980	0.981
$q_7 [deg]$	0	0	0	0	-	-	-	-
$q_{11} [deg]$	9.21	9.49	9.12	8.99	0.982	0.974	0.979	0.978
$q_{12} [deg]$	6.03	6.14	5.71	5.47	0.993	0.993	0.993	0.993
$q_{13} [deg]$	16.78	17.15	16.70	16.76	0.990	0.986	0.994	0.989
$q_{14} [deg]$	7.49	8.85	6.40	7.69	0.990	0.987	0.991	0.989
$q_{15} [deg]$	0	0	0	0	-	-	-	-

4.4. Real Test Results

To assess our algorithm performance against real data from motion capture, we compare the positions of the participant's elbows, shoulders and wrists expressed in the rowing global reference frame ($S_0 = [x_0, y_0, z_0]$), conveniently aligned with the motion capture global reference system. For each position we define $\check{p} = (\check{x}, \check{y}, \check{z})^T$ the algorithm estimation and $\tilde{p} = (\tilde{x}, \tilde{y}, \tilde{z})^T$ the variables reconstruction from optical data. The measures employed is RMSE and correlation coefficient.

The results of the real tests are reported in Table 6. Table 6 reports the RMSEs against optical data and the correlation coefficient between the trajectories for every position considered, i.e.: right shoulder (p_{ShR}), left shoulder (p_{ShL}), right elbow (p_{ElR}), left elbow (p_{ElL}), right wrist (p_{WrR}), left wrist (p_{WrL})

Table 6. RMSE for the positions expressed in meters, and the correlation coefficient, over a period of 40s.

Position	RMSE [m]	r
p_{ShR}	0.078	0.3965
p_{ShL}	0.081	0.4814
p_{ElR}	0.158	0.8299
p_{ElL}	0.153	0.9081
p_{WrR}	0.034	0.9913
p_{WrL}	0.054	0.9864

We also report the comparison between of our algorithm and the optical tracking system in Figure 4 and 5 to show how the algorithm performs.

5. Discussion

Results from the simulated data show that for typical values of the boat acceleration the motion reconstruction is minimally affected by the boat motion (the error increases 3.32% on average). The estimation is more affected, from this point of view, by erroneous estimation of the biases. Results show also that the accuracy of the reconstruction is comparable to state of the art results (see [16], [23] and [15]) obtained when the trunk of the tracked person is steady. The only remarkable difference between simulated and estimated joint variables is for the q_2 joint. As it can be seen from Figure 3 the estimated value is shifted with respect to the ground truth. This may be due to the simplified back model.

In the real test case the position placement is matched with varying precision, higher on the wrists, with increasing correlation from the shoulder to the wrist as expected from the closed kinematics. The right shoulder position along x axis is not tracked correctly due to the reduced number of sensors involved.

Overall, the results from both cases show a good capability of the system to reconstruct the motion of the rower. In both cases the estimation provides useful data for scoring the user performance in terms of technique features. Examples of technique features that can be evaluated only if the trunk and the upper limbs are tracked are the back leaning and the orientation of the plane defined by the upper arm and the forearm ([24], [25]) during the finish phase (i.e. when legs are stretched and oars are pulled by means of the arms action, see [26] for further details). Our algorithm provides back leaning as q_2 and allows to evaluate the finish phase by checking q_3 to q_7 and q_{11} to q_{15} . These features are typically visually inspected by coaches and require motion tracking that may be difficult to be performed with optical techniques in indoor rowing and even impractical in outdoor rowing.

Results support using our methods for both in-door and out-door rowing. For the latter case we have shown the introduction of the effect of forward boat acceleration that has minimal effects on estimated motion. One open aspect of transferring the presented algorithm to the outdoor rowing case is the angular velocity. In this case there are fewer data in the literature to support early considerations. However, these data (see [27] and [28]) suggest that angular velocity of the shell is much lower than that of the limbs: boat pitch, roll and yaw variation within a stroke (a rowing cycle) are less than 1° , 5° and 5° respectively and sum to zero within a stroke except for yaw, whose contribution actually depends on the desired boat trajectory. Results from simulated data support this thesis. However, shell acceleration and its angular velocity can be accounted for by means of an IMU placed on the rower's waist.

The possibility of application of the proposed approach in outdoor rowing settings raises the question of computational cost. Analyzing the various steps involved in the kinematic reconstruction it is possible to extract a O-notation of the overall computational cost:

$$O(m^3 + nm^2 + mn^2 + n^3 + nf + ns) \quad (19)$$

Where n the number of state variables connected to the number of joints; f the total number of frames that depend on the joints and on the structure; s as the total number of inertial sensors and m the number of observed variables that depends on the sensors. In the specific case of the experimental assessment these values are $n = 37$, $f = 25$, $s = 5$ and $m = 58$. The execution of the reconstruction, implemented in C code as generated from Simulink, running on a Intel Core i7 2.66 GHz M620 (nominal 21.3 giga FLOPs per core), produces an average rate of 116 steps per second (approx 707 MFLOPs).

The algorithm can take advantage of parallel execution in particular when performing the evaluation of the $h(\cdot)$ for each of the $2n + 1$ sigma points. Due to the number of items involved in the example case (75) this operation can take advantage of GPU computing. The recent advancements of mobile GPU open the possibility of using this algorithm in real-time in a wearable system.

6. Conclusion

This paper showed a novel approach to track outdoor rowing performance based on the fusion of data gathered from the device and body motion data obtained from inertial sensors. The method showed to provide useful data for indoor rowing performance assessment and its extension to outdoor rowing was discussed to motivate how the validation proposed in this paper could be extended to the outdoor rowing case. The test of the method in outdoor rowing will be approached in a future work to confirm the statements we made in the discussion section. Additional directions for investigation are the reduction of computational complexity by decomposing the problem through graphical models [17] and the introduction of constraints such as human joint limits.

References

- [1] Ruffaldi E, Filippeschi A, Avizzano CA, Bardy B, Gopher D, Bergamasco M. Feedback, affordances, and accelerators for training sports in virtual environments. *Presence: Teleoperators and Virtual Environments*. 2011;20(1):33–46.
- [2] Rauter G, Sigrist R, Koch C, Crivelli F, van Raaij M, Riener R, et al. Transfer of Complex Skill Learning from Virtual to Real Rowing. *PLoS ONE*. 2013 12;8(12):e82145. Available from: <http://dx.doi.org/10.1371/journal.pone.0082145>.
- [3] Barris S, Button C. A review of vision-based motion analysis in sport. *Sports Medicine*. 2008;38(12):1025–1043.
- [4] Filippeschi A, Ruffaldi E. Boat Dynamics and Force Rendering Models for the SPRINT System. *Human-Machine Systems, IEEE Transactions on*. 2013;43(6):631–642.
- [5] Vlasic D, Adelsberger R, Vannucci G, Barnwell J, Gross M, Matusik W, et al. Practical motion capture in everyday surroundings. *ACM Transactions on Graphics (TOG)*. 2007;26(3):35.
- [6] Bleser G, Hendeby G, Miezal M. Using egocentric vision to achieve robust inertial body tracking under magnetic disturbances. In: *Mixed and Augmented Reality (ISMAR), 2011 10th IEEE International Symposium on*. IEEE; 2011. p. 103–109.
- [7] Gravenhorst F, Thiem C, Tessedorf B, Adelsberger R, Arnrich B, Draper C, et al. SonicSeat: design and evaluation of a seat position tracker based on ultrasonic sound measurements for rowing technique analysis. *Journal of Ambient Intelligence and Humanized Computing*. 2014;p. 1–10. Available from: <http://dx.doi.org/10.1007/s12652-013-0216-5>.
- [8] Gravenhorst F, Turner T, Draper C, Smith RM, Troester G. Validation of a Rowing Oar Angle Measurement System Based on an Inertial Measurement Unit. In: *Trust, Security and Privacy in Computing and Communications (TrustCom), 2013 12th IEEE International Conference on*. IEEE; 2013. p. 1412–1419.

-
- [9] Tessendorf B, Gravenhorst F, Arnrich B, Troster G. An imu-based sensor network to continuously monitor rowing technique on the water. In: *Intelligent Sensors, Sensor Networks and Information Processing (ISSNIP), 2011 Seventh International Conference on*. IEEE; 2011. p. 253–258.
- [10] Hoffmann CP, Filippeschi A, Ruffaldi E, Bardy BG. Energy management using virtual reality improves 2000-m rowing performance. *Journal of Sports Sciences*. 2013;0(0):1–9. PMID: 24053155. Available from: <http://www.tandfonline.com/doi/abs/10.1080/02640414.2013.835435>.
- [11] Zhu R, Zhou Z. A real-time articulated human motion tracking using tri-axis inertial/magnetic sensors package. *Neural Systems and Rehabilitation Engineering, IEEE Transactions on*. 2004;12(2):295–302.
- [12] Yun X, Bachmann ER. Design, implementation, and experimental results of a quaternion-based Kalman filter for human body motion tracking. *Robotics, IEEE Transactions on*. 2006;22(6):1216–1227.
- [13] Cheng Y, Shuster MD. Robustness and Accuracy of the QUEST Algorithm. *Advances in the Astronautical Sciences*. 2007;127:41–61.
- [14] Roetenberg D, Luinge H, Slycke P. Xsens MVN: full 6DOF human motion tracking using miniature inertial sensors; 2009.
- [15] El-Gohary M, McNames J. Shoulder and Elbow Joint Angle Tracking With Inertial Sensors. *Biomedical Engineering, IEEE Transactions on*. 2012;59(9):2635–2641.
- [16] Peppoloni L, Filippeschi A, Ruffaldi E, Avizzano CA. A novel 7 degrees of freedom model for upper limb kinematic reconstruction based on wearable sensors. In: *Intelligent Systems and Informatics (SISY), 2013 IEEE 11th International Symposium on*. IEEE; 2013. p. 105–110.
- [17] Ruffaldi E, Peppoloni L, Filippeschi A, Avizzano CA. A novel approach to motion tracking with wearable sensors based on Probabilistic Graphical Models. In: *Robotics and Automation, ICRA. The IEEE International Conference on*. IEEE. IEEE; 2014. p. 1247–1252.
- [18] Wan EA, Van Der Merwe R. The unscented Kalman filter for nonlinear estimation. In: *Adaptive Systems for Signal Processing, Communications, and Control Symposium 2000. AS-SPCC. The IEEE 2000*. IEEE; 2000. p. 153–158.
- [19] Denavit J. A kinematic notation for lower-pair mechanisms based on matrices. *Trans of the ASME Journal of Applied Mechanics*. 1955;22:215–221.
- [20] Ruffaldi E, Sandoval-Gonzalez O, Filippeschi A, Tripicchio P, Frisoli A, Avizzano C, et al. Integration of multimodal technologies for a rowing platform. In: *Mechatronics, ICM. The IEEE International Conference on*. IEEE; 2009. p. 1–6.
- [21] Frisoli A, Ruffaldi E, Bagnoli L, Filippeschi A, Avizzano CA, Vanni F, et al. Preliminary design of rowing simulator for in-door skill training. In: *Proceedings of the 2008 Ambi-Sys workshop on Haptic user interfaces in ambient media systems. ICST (Institute for Computer Sciences, Social-Informatics and Telecommunications Engineering); 2008*. p. 9.
- [22] Tolani D, Goswami A, Badler NI. Real-time inverse kinematics techniques for anthropomorphic limbs. *Graphical models*. 2000;62(5):353–388.
- [23] Zhang ZQ, Wong WC, Wu JK. Ubiquitous human upper-limb motion estimation using wearable sensors. *Information Technology in Biomedicine, IEEE Transactions on*. 2011;15(4):513–521.
- [24] Fothergill S, Harle R, Holden S. Modeling the model athlete: Automatic coaching of rowing technique. In: *Structural, Syntactic, and Statistical Pattern Recognition*. Springer; 2008. p. 372–381.
- [25] Filippeschi A, Ruffaldi E. Expert rowers’s motion analysis for synthesis and technique digitalization. In: *BIO Web of Conferences*. vol. 1. EDP Sciences; 2011. p. 00024.
- [26] Nolte V. Rowing faster. *Human Kinetics*; 2011.
- [27] Mola A. Multiphysics and multilevel fidelity modeling and analysis of Olympic rowing boat dynamics. Virginia Polytechnic Institute and State University; 2010.
- [28] Formaggia L, Miglio E, Mola A, Montano A. A model for the dynamics of rowing boats. *International journal for numerical methods in fluids*. 2009;61(2):119–143.

List of Figures

- 1 Visual representation of the kinematic model depicted in the neutral pose (N-pose). The upper body of the rower is represented on the seat that moves on a rail. In the same picture the two oars are represented along with the boxes that hold them. The root reference system is placed on the seat rail having Z toward the oars, Y pointing upwards and X pointing towards the left oar. In this representation the rotoidal joints are shown as cylinders, while spherical joints are shown as balls. These joints are connected by links as solid thick lines. The parameters that are required for the kinematic model are represented as well except for $r_{0,18}^0$ and $r_{0,22}^0$. The frames are grouped according to the joint they are related to. The origins of each joint group are in the center of the joint (e.g. frames #2 to #4 origins are in the humerus head). 15
- 2 Photo of the experimental setup showing the rower over the SPRINT system. The system is surrounded by Vicon motion capture cameras for validation. The user is wearing the inertial units and motion capture markers. Each inertial unit is also associated with a marker for validating the motion tracking in position in addition to joint angles. 16
- 3 Comparison between simulated and estimated joint variables of the rower real motion (Back, Shoulder, Wrists). Solid lines are the result of the estimation whereas dashed lines are the synthetic data that represents the rower motion. The negative values of the elbow flexion depend upon the definition of the elbow reference frame, namely frames 6 and 14 in the DH chain. The synthetic data show no extension, while a little extension (positive values) is estimated by the system, since no constraints are imposed on the estimated joint angles. 17
- 4 Motion tracking results obtained with the inertial tracking system algorithm for the first rowing trial (Shoulder and Elbow frames). Solid lines are the result of the estimation whereas dashed lines are the synthetic data that represents the rower motion. These are reported only for the right arm due to the symmetry of the results. The positions are represented in the world reference frame, which is centered in the origin of the seat sliding guide, with x pointing towards the rower's feet and y pointing upward, as shown in Figure 1. 18
- 5 Motion tracking results obtained with the inertial tracking system algorithm for the first rowing trial (Wrist frame). Solid lines are the result of the estimation whereas dashed lines are the synthetic data that represents the rower motion. Only right arm has been reported for compactness of presentation. These positions are expressed in the global frame in the same way of Figure 4. 19



Fig. 2. Photo of the experimental setup showing the rower over the SPRINT system. The system is surrounded by Vicon motion capture cameras for validation. The user is wearing the inertial units and motion capture markers. Each inertial unit is also associated with a marker for validating the motion tracking in position in addition to joint angles.

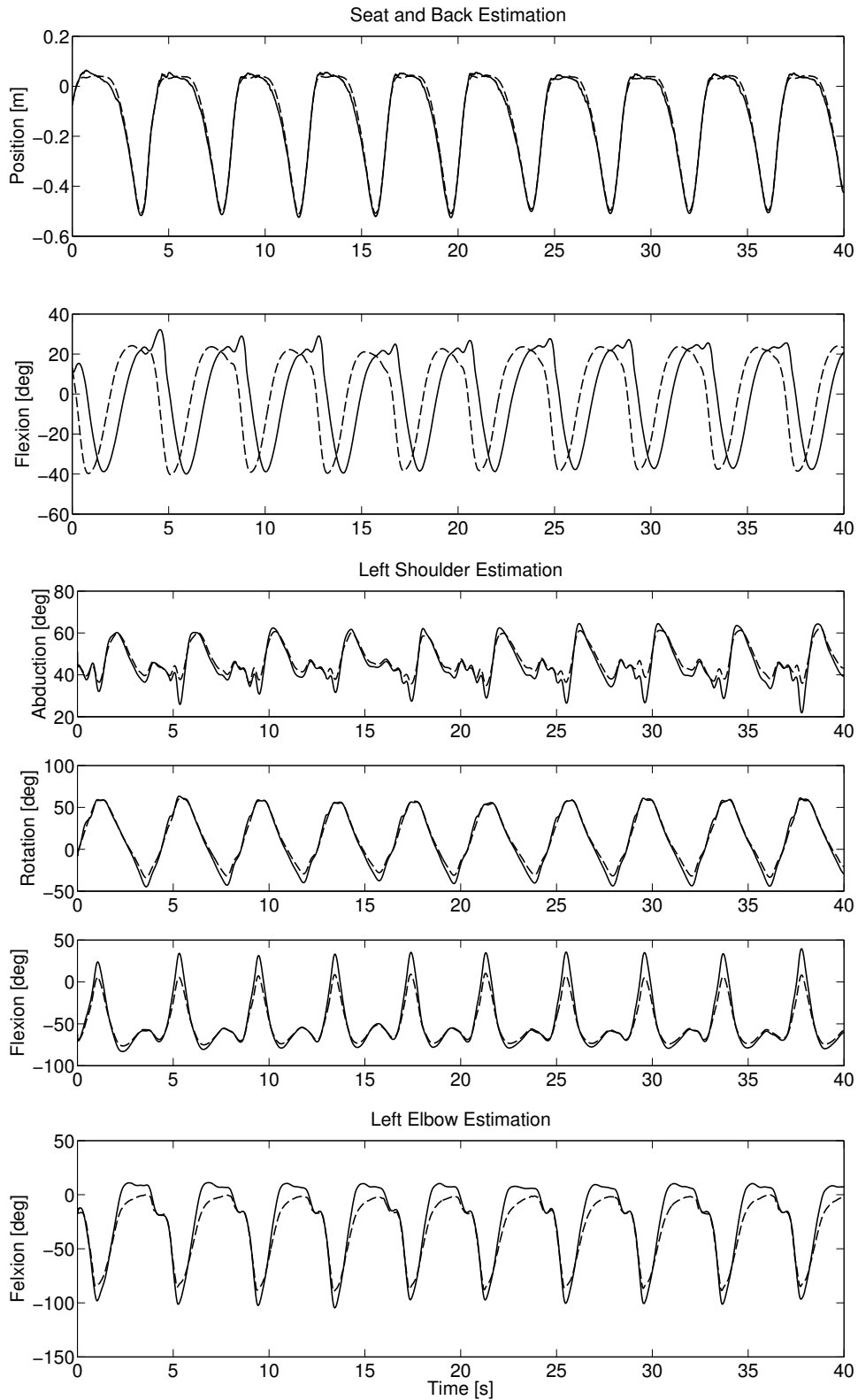


Fig. 3. Comparison between simulated and estimated joint variables of the rower real motion (Back, Shoulder, Wrists). Solid lines are the result of the estimation whereas dashed lines are the synthetic data that represents the rower motion. The negative values of the elbow flexion depend upon the definition of the elbow reference frame, namely frames 6 and 14 in the DH chain. The synthetic data show no extension, while a little extension (positive values) is estimated by the system, since no constraints are imposed on the estimated joint angles.

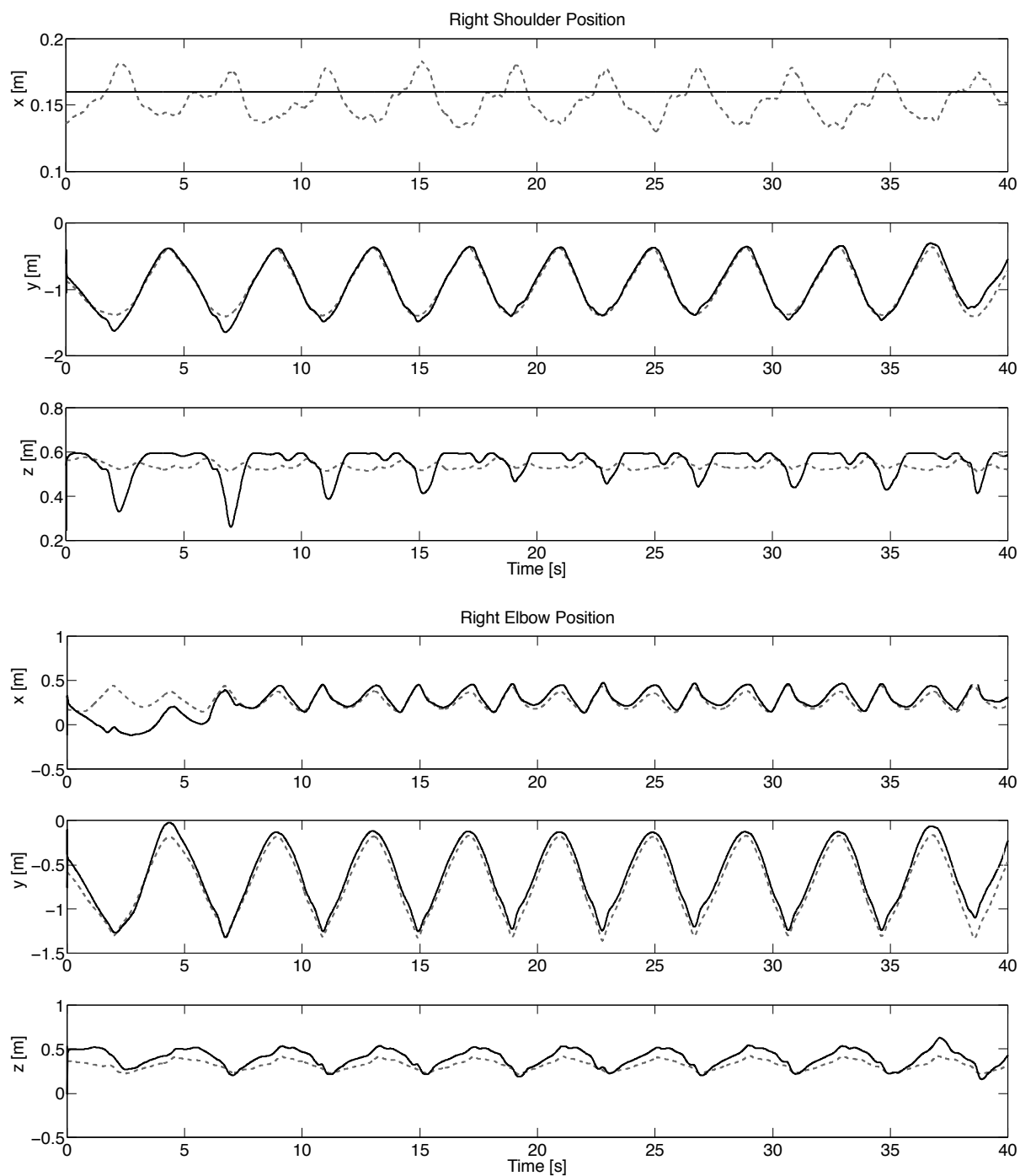


Fig. 4. Motion tracking results obtained with the inertial tracking system algorithm for the first rowing trial (Shoulder and Elbow frames). Solid lines are the result of the estimation whereas dashed lines are the synthetic data that represents the rower motion. These are reported only for the right arm due to the symmetry of the results. The position are represented in the world reference frame, which is centered in the origin of the seat sliding guide, with x pointing towards the rower's feet and y pointing upward, as shown in Figure 1.

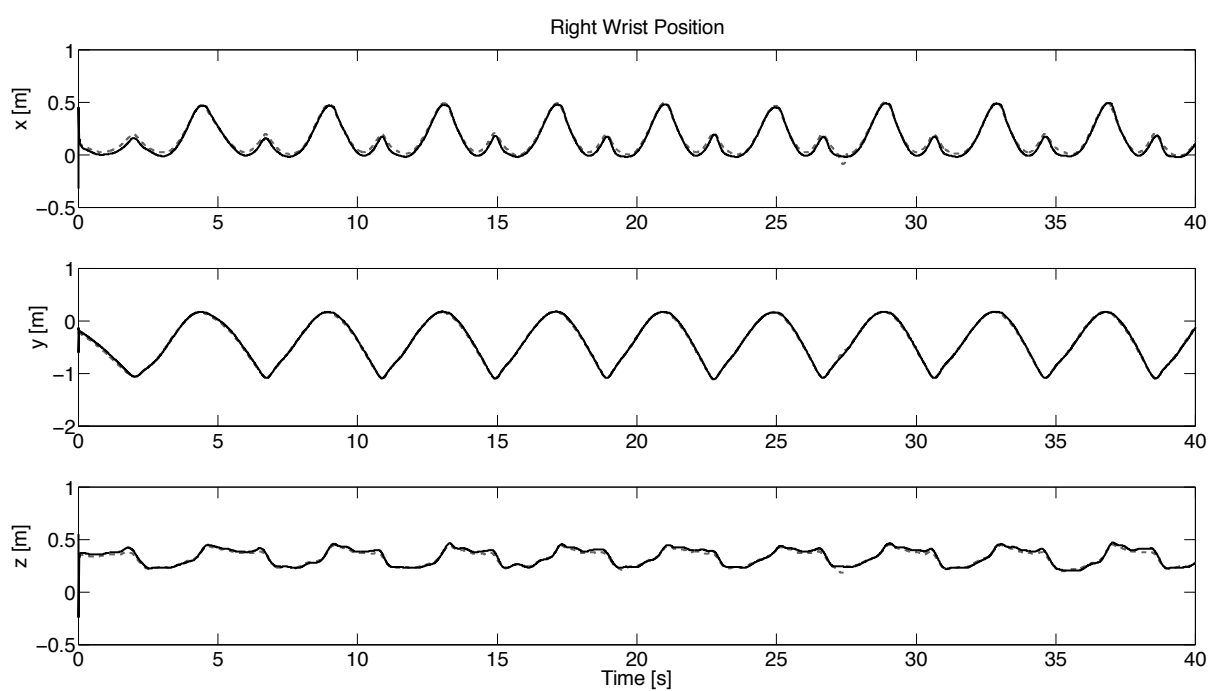


Fig. 5. Motion tracking results obtained with the inertial tracking system algorithm for the first rowing trial (Wrist frame). Solid lines are the result of the estimation whereas dashed lines are the synthetic data that represents the rower motion. Only right arm has been reported for compactness of presentation. These positions are expressed in the global frame in the same way of Figure 4.